Physica B 503 (2016) 126–129

Contents lists available at ScienceDirect

Physica B

journal homepage: www.elsevier.com/locate/physb

Influences of Stone–Wales defects on the structure, stability and electronic properties of antimonene: A first principle study

Yonghong Hu[a,*,1], Yunyi Wu[b,1], Shengli Zhang[c]

[a] School of Nuclear Technology and Chemistry & Biology, Hubei University of Science and Technology, Xianning 437100, PR China
[b] Department of Energy Materials and Technology, General Research Institute for Nonferrous Metals, Beijing, China
[c] Institute of Optoelectronics & Nanomaterials, Herbert Gleiter Institute of Nanoscience, College of Materials Science and Engineering, Nanjing University of Science and Technology, Nanjing 210094, PR China

ARTICLE INFO

Keywords:
Antimonene
Stone–Wales defect
Electronic properties
2D semiconductors
Density functional calculations

ABSTRACT

Defects are inevitably present in materials, and their existence strongly affects the fundamental physical properties of 2D materials. Here, we performed first-principles calculations to study the structural and electronic properties of antimonene with Stone–Wales defects, highlighting the differences in the structure and electronic properties. Our calculations show that the presence of a SW defect in antimonene changes the geometrical symmetry. And the band gap decreases in electronic band structure with the decrease of the SW defect concentration. The formation energy and cohesive energy of a SW defect in antimonene are studied, showing the possibility of its existence and its good stability, respectively. The difference charge density near the SW defect is explored, by which the structural deformations of antimonene are explained. At last, we calculated the STM images for the SW defective antimonene to provide more information and characters for possible experimental observation. These results may provide meaningful references to the development and design of novel nanodevices based on new 2D materials.

1. Introduction

Two-dimensional materials (2D), such as grapheme, silicene, hexagonal boron nitride, molybdenum disulfide, phosphorene and germanene et al., have received increasing attention recently owing to their unique properties and promising applications [1–16]. Recently, two new ultrathin 2D semiconductor materials in group-V, namely, arsenene and antimonene, have been firstly estimated to be stably exists, which may also promote the development of 2D semiconductor-based optoelectronic devices, such as blue and UV light-emitting diodes and photodetectors. Arsenene and antimonene, as a new 2D materials, have received great attentions [17].

Defects are often inevitable in the fabrication and processing of the monolayer materials, such as vacancies, adatoms, and topological defects, which may impact significantly the electronic and chemical properties of nanomaterials [1–11]. Stone–Wales (SW) defect [18] is a well-known example, which is comprised of two pairs of five-membered and seven-membered rings formed by rotating one bond of the traditional six-membered ring by 90°. SW-defects have been extensively studied in graphene [19–23]. It has been experimentally formed by isolating graphene on a silicon wafer through mechanical cleavage and is observed in situ [24]. These defects have been known to alter mechanical as well as electronic properties, thereby finding possible attractive applications in the semiconductor industry. The effect of SW defects on the electronic and mechanical properties of carbon nanotubes (CNTs), BN nanotubes (BNNTs), and GNRs has drawn considerable attention [25–38]. It's shown that the SW defects play an important role in the structural, electronic and chemical properties of various kinds of 2D nanomaterials. To the best of our knowledge, however, there are still no investigations on the structural and electronic properties of antimonene with SW defects.

In the present work, we study the geometrical structures and electronic property of the SW defects in antimonene sheet using the density functional theory calculations. We find that the SW defect significantly influences the structural and electronic properties of antimonene, and that the content of SW defect plays an important role. A ripple in antimonene sheet is created when the SW defect is introduced, and all the optimized structures of antimonene containing a SW defect possess center symmetry. The formation energy and cohesive energy of a SW defect in antimonene are calculated and compared with that of the SW defect in silicene, indicating excellent stability. It is found that the SW defected antimonene becomes direct

* Corresponding author.
E-mail address: hchyh2001@tom.com (Y. Hu).
[1] These authors contributed equally to this work.

http://dx.doi.org/10.1016/j.physb.2016.08.034
Received 20 July 2016; Accepted 21 August 2016
Available online 22 August 2016

band gap semiconductor. To further understand the variations of geometrical structure and electronic property, we calculated the difference charge density and STM images of antimonene with a SW defect. Our researches may provide valuable insights into the identification of SW defect in further experiments and the understanding their effects on the properties and applications of antimonene.

2. Computational methods

All of our calculations, including geometry relaxation and energy calculations were performed using the Cambridge Sequential Total Energy Package (CASTEP) with a norm-conserving pseudo-potential [39]. The exchange- correlation functional is treated using a generalized gradient approximation (GGA) according to Perdew–Wang exchange-correlation functional (PW91) [40]. The periodic boundary condition is used to simulate infinite antimonene sheets with and without SW defect. A sufficiently large 20 Å vacuum region is used to separate the 2D structures to rule out any interaction among the neighboring layers along *z*-axis. The structure is optimized by means of the Broyden-Fletcher-Goldfarb-Shanno (BFGS) method [41]. The basis set of valence electronic states is set to be $5s^25p^3$ for Sb. All of the structure models were fully relaxed until the forces were smaller than 0.01 eV $Å^{-1}$. The self-consistent convergence is set at 5×10^{-6} eV per atom. The plane wave basis set with a cutoff energy of 330 eV is adopted. As for the Brillouin-zone sampling, we use the Monkhorst-Pack mesh with 7×7×1 *k*-points [42]. To simulate different SW defect concentrations (i.e.,6.25–1.39%), the supercell size was varied from 3×3 to 6×6 with one SW defect in the supercell. With increasing supercell size, the concentration effectively decreases. Brillouin zone integrations were carried out over a 7×7×1 mesh of k points for a 6×6×1 supercell. In order to minimize the interactions between the neighboring SW defects, for the calculation of electronic properties, we employed a large supercell derived from a 6×6 supercell of antimonene.

3. Results and discussion

3.1. Geometric properties of SW-defected antimonene

Various defects always exist in crystals, so it's very necessary to understand their effects on the structural and electronic characteristics of materials. SW defect is one of the most common defects that have been observed in low-dimensional materials. Therefore, it may exist in the antimonene nanosheet. The fully relaxed antimonene supercell with a SW defect is shown in Fig. 1. As can be seen from Fig. 1, the antimonene with SW-defect maintains its buckled two-dimensional structure with obvious local out-of-plane displacements of the Sb atoms near the SW defect. After the creation of the SW defect, the Sb–Sb bond between the dimmer becomes stronger and its length changes from 2.76 to 2.70 A°, the Sb–Sb bond near the dimmer becomes weaker than in defect-free antimonene and their lengths increase from 2.7 to about 2.8 A° (see Table S1 in the supporting materials). The lattice constant increases from 22.12 to 23.64 A° for the 6×6×1 supercell. The Sb atoms favor buckled configuration in bare antimonene, and a ripple perpendicular to the sheet along the direction from Sb-5 to Sb-11 is created when the SW defect is introduced. It's found that the optimized structure of antimonene containing a SW defect in Fig. 1 retains a particular symmetry. The Sb atoms labeled "0" and "3" in the SW defect are at the equivalent positions relative to the center of the SW defect, which is at the middle point between the two Sb atoms labeled "1" and "2". Because of the center symmetry of the optimized structure, there are many other Sb atoms at equivalent positions, such as the Sb atom pairs labeled "4" and "10″, "5" and "11″, "6" and "12″, "7" and "13″ etc. This geometrical property is obviously different from those of the SW defective sillicene and graphene. The structural and electronic properties for bare antimonene and SW-defected antimonene with different SW defect content are given in Table 1. The calculated structural parameters (a, d_{Sb-Sb} and α) in Table 1 all change monotonously with the SW defect content, indicating that the larger supercell case is more close to the pure antimonene. Hence, in the following study, the $6\times6\times1$ supercell of antimonene sheet with a single SW defect is taken as a typical example.

3.2. Formation and stability of Stone–Wales defect in antimonene

It is well known that SW defect may be formed during the growth process or under irradiation. Now we investigate the formation energy and stability of SW defects in antimonene. Compared to graphene and silicene, the interatomic distance in antimonene is larger [22]. Perfect antimonene has buckled hexagonal lattice structure, so the SW defect is easy to be introduced. The formation energy of a SW defect in antimonene is given by $E_f = E_{Ant}^{SW} - E_{Ant}$, where E_{Ant}^{SW} and E_{Ant} are the total energies of antimonene with a SW defect and defect-free antimonene, respectively. According to this formula, the formation energy of a SW defect in a 6×6×1 antimonene supercell is calculated to be 1.36 eV, which is even lower than that of a SW defect in silicene (E_f = 1.64 eV). Additionally, the stability of antimonene with SW defect can also be predicted via its cohesive energy. The cohesive energy is defined as $E_{coh} = (E_{Tot}/N) - E_a$, where E_{Tot} and E_a are the total energy of the whole system and an isolated atom, respectively. N is the number of atoms in the supercell. According to this equation, the cohesive energies of antimonene and SW-defected antimonene are calculated to be −4.58 and −4.56 eV, respectively. The common negative values of the cohesive energies indicate that they both have good stability. As seen from Table 1, the formation energy and cohesive energy of the antimonene sheet with a single SW defect both decrease monotonously with the decrease of SW defect content, changing towards the values of the pure antimonene. Therefore, these calculations are self-consistent and reliable.

3.3. Electronic properties of Stone–Wales defect in antimonene

Sb is typical semimetals in the bulk, while antimonene is reported to be an indirect semiconductor with band gap of 2.28 eV [17]. The conduction-band-bottom of the antimonene mainly consists of Sb 5p states coupled with small amounts of Sb 5 s states. The six Sb 5p states split into three bonding and three antibonding states forming a band gap around the Fermi level. In pure antimonene, there are three s-bonding orbitals and a lone pair of electrons, which decline to form π-type bonding states [17]. In Fig. 2, the electronic band dispersion

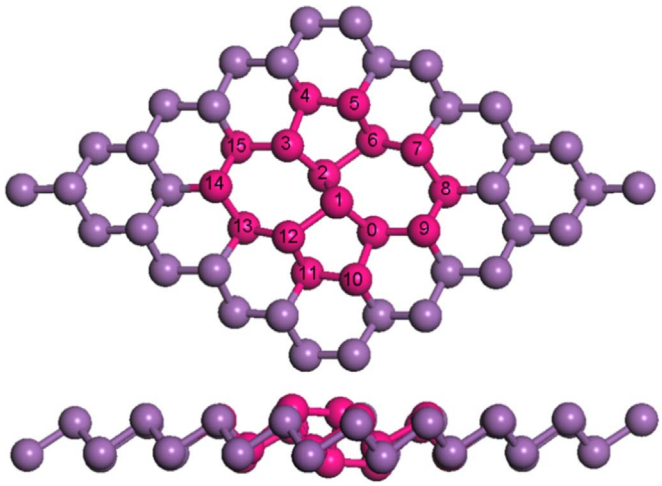

Fig. 1. The top and side views of the fully relaxed antimonene with a Stone–Wales defect. All the spheres represent Sb atoms and the pink spheres represent the most related Sb atoms to SW defect. (For interpretation of the references to color in this figure legend, the reader is referred to the web version of this article.)

Table 1
Calculated structural and electronic properties for pure antimonene and SW-defected antimonene: lattice parameter (a), Sb–Sb distance (d_{Sb-Sb}), angle between two of the lattice vectors of the supercell (α), formation energy (E_f), cohesive energy (E_{coh}), and the band gap (E_{gap}).

		a Å	d_{Sb-Sb} Å	α deg	E_f eV	E_{coh} eV	E_{gap} eV
Antimonene	6 × 6 × 1	22.12	2.76	60.00	0.00	−4.58	1.84
SW-antimonene	6 × 6 × 1	23.64	2.70–2.84	60.37	1.36	−4.56	1.45
	5 × 5 × 1	19.70	2.70–2.85	60.56	1.37	−4.55	1.42
	4 × 4 × 1	15.72	2.70–2.86	62.45	1.49	−4.54	1.59
	3 × 3 × 1	11.82	2.69–2.88	63.11	1.65	−4.48	0.92

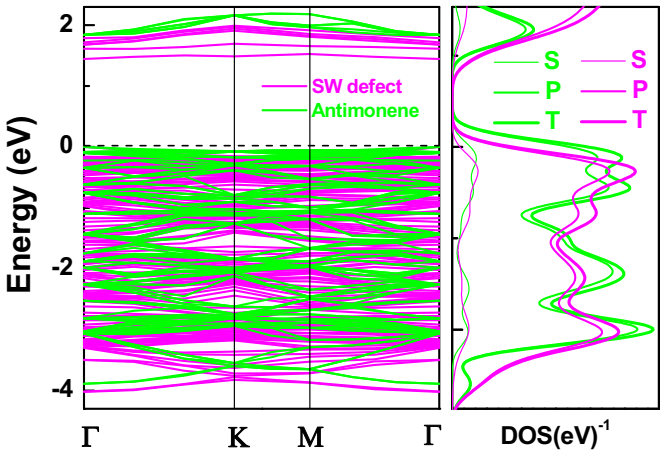

Fig. 2. Band structures and PDOS of the 6 × 6 antimonene with and without a SW defect.

and corresponding densities of states of the perfect and SW-defected antimonene for 6 × 6 supercells are presented. It is noted that both the valence bands and conduction bands shift toward low energy range after the creation of a SW defect. Although the calculated energy band gap decreases from 1.84 to 1.45 eV, its energy band structure remains showing a direct band gap. It can be seen from Table 1 that the energy band gap of the antimonene sheet with a single SW defect increases with the decrease of SW-defect content. Here the calculated values of energy band gaps are lower than that previously reported value (2.28 eV) due to the different accuracy between GGA and HSE methods, however, the variation trend of the energy band gap versus SW defect content is correct without extra influence. The partial and total densities of states of the perfect and SW-defected antimonene are also studied, which are in consistent with the variations of the electronic band structures. Before and after the creation of a SW defect

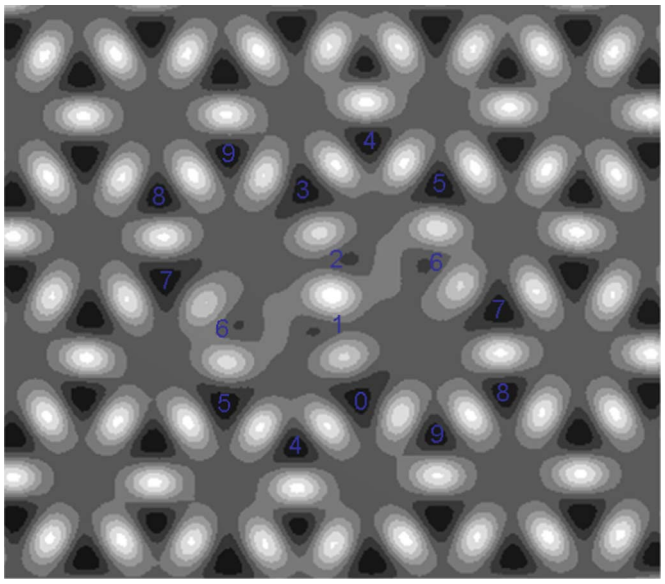

Fig. 4. The slicing plane (parallel to the antimonene sheet and through the center of SW defect) of the charge differences optical spectrums of antimonene with a SW defect.

in antimonene sheet, both the maximum of the valence band and the minimum of the conduction band mainly composed of the p orbital of Sb atoms.

To gain further insights, we also computed the density of states and the electron density isosurfaces for both the valence band maximum (VBM) and the conduction band minimum (CBM) of the antimonene with a SW defect as shown in Fig. 3. Both the VBM and CBM of antimonene are combinations of mainly p atomic orbital.

As a result of local deformations induced by the presence of a SW defect, the charge differences optical spectrums of the antimonene with a SW defect is found to be much different as shown in Fig. 4. In Fig. 4, the positions of the Sb atoms are indicated by the natural numbers, which are in consistent with the top view part in Fig. 1. It is found that the difference charge density ($\rho_\uparrow - \rho_\downarrow$) around the Sb atoms "1", "2" and "6" are obviously different from the others. The variations of the contour of the difference charge density of these Sb atoms is induced by the variations of the corresponding Sb–Sb bond lengths.

3.4. STM image of Stone–Wales defect in antimonene

To help recognize the SW defect in antimonene in future experiments, the scanning tunneling microscopy (STM) image of antimonene with SW defect is simulated at 1.0 V bias as shown in Fig. 5. At positive bias (+1.0 V), the STM image of SW defect is easy to understand and correlate with its defective atom structure.

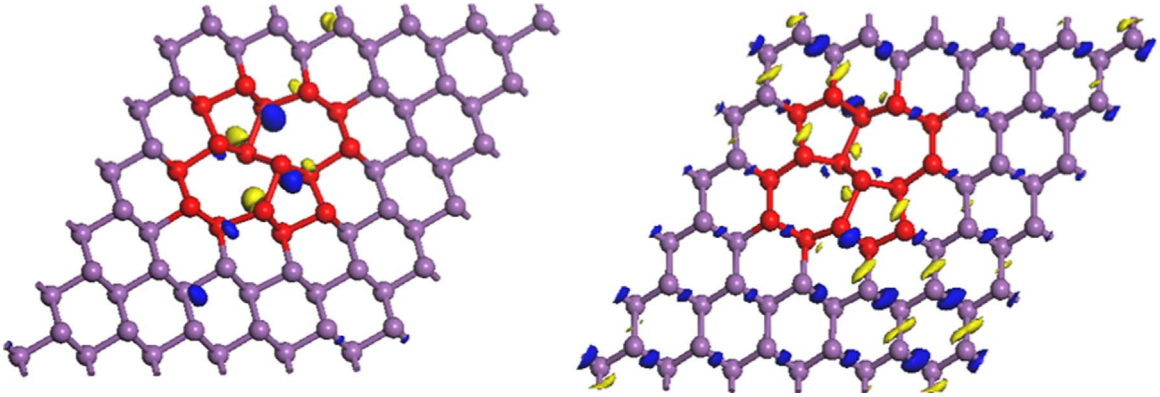

Fig. 3. Electron density isosurfaces of the highest-energy valence (left part) and the lowest-energy conduction (right part) bands of the antimonene with a SW defect.

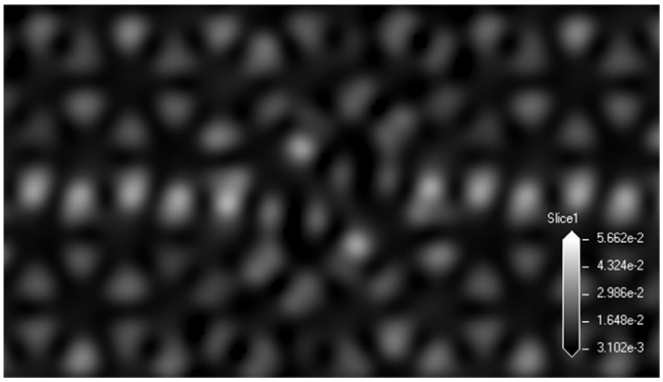

Fig. 5. STM profile with positive bias 1 V.

4. Conclusions

Here the ab initio calculations are perfumed to investigate the formation of SW defects in antimonene and their effects on electronic properties. The formation energy of the SW defect in the buckled lattice structure of antimonene with a large supercell ($6 \times 6 \times 1$) is found to be 1.36 eV, which is even lower than those of SW-defects in silicene and grapheme. The calculation results of formation energy and cohesive energy both help us a lot to understand the softer bonding nature of antimonene, which results in easier formation of a SW defect for freestanding antimonene. The introduction of a SW defect in antimonene breaks the original symmetry and results in a band gap decrease in electronic band structure. It's found that the structural and electronic properties of SW-defected antimonene are dependent to the defect concentration or supercell size. The calculation result of difference charge density reveals that the formation of SW defects in freestanding antimonene inevitably leads to the deformations. Additionally, we provide the STM image of the SW-defected antimonene, which can help us to recognize the SW defect in future experiments about antimonene sheet. Our results help us to well understand the characteristic properties of defected antimonene, which are important for the applications of antimonene in future low-dimensional electronics.

Acknowledgments

This work was supported by the NSFC (61222403, 11274173, 51402020) and the Doctoral Program Foundation of China (20123218110030). We also acknowledge Computer Network Information Center (Supercomputing center) of Chinese Academy of Sciences (CAS) for allocation of computing resource.

Appendix A. Supporting information

Supplementary data associated with this article can be found in the online version at doi:10.1016/j.physb.2016.08.034.

References

[1] A.H.C. Neto, F. Guinea, N.M.R. Peres, K.S. Novoselov, A.K. Geim, Rev. Mod. Phys. 81 (2009) 109.
[2] S.D. Sarma, S. Adam, E.H. Hwang, E. Rossi, Rev. Mod. Phys. 83 (2011) 407.
[3] M.S. Xu, T. Liang, M.M. Shi, H.Z. Chen, Chem. Rev. 113 (2013) 3766.
[4] W.F. Tsai, C.Y. Huang, T.R. Chang, H. Lin, H.T. Jeng, A. Bansil, Nat. Commun. 4 (2013) 1.
[5] S. Lebegue, O. Eriksson, Phys. Rev. B 79 (2009) 115409.
[6] K.F. Mak, C. Lee, J. Hone, J. Shan, T.F. Heinz, Phys. Rev. Lett. 105 (2010) 136805.
[7] M. Ezawa, Phys. Rev. Lett. 109 (2012) 055502.
[8] X.D. Zhang, Y. Xie, Chem. Soc. Rev. 42 (2013) 8187.
[9] L. Li, Y. Yu, Y. Zhang, et al., Nat. Nanotechnol. 9 (2014) 372.
[10] F. Xia, H. Wang, Y. Jia, Nat. Commun. 5 (2014) 4458.
[11] M. Buscema, D.J. Groenendijk, G.A. Steele, et al., Nat. Commun. 5 (2014) 4651.
[12] E.S. Reich, Nature 506 (2014) 19.
[13] Y. Hu, S. Zhang, S. Sun, M. Xie, B. Cai, H.B. Zeng, Appl. Phys. Lett. 107 (2015) 122107.
[14] S. Zhang, Y. Hu, Z. Hu, B. Cai, H.B. Zeng, Appl. Phys. Lett. 107 (2015) 022102.
[15] S. Zhang, M. Xie, F. Li, H.B. Zeng, et al., Angew. Chem. Int. Ed. 55 (2016) 1666.
[16] S. Zhang, M. Xie, B. Cai, H.B. Zeng, et al., Phys. Rev. B 93 (2016) 245303.
[17] S. Zhang, Z. Yan, Y. Li, Z. Chen, H.B. Zeng, Ange. Chem. Inter. Ed. 54 (2015) 3112.
[18] A. Stone, D. Wales, Chem. Phys. Lett. 128 (1986) 501.
[19] A. Manjanath, A.K. Singh, Chem. Phys. Lett. 592 (2014) 52.
[20] F. Banhart, J. Kotakoski, A.V. Krasheninnikov, ACS Nano 5 (2011) 26.
[21] G.G. Samsonidze, G.G. Samsonidze, B.I. Yakobson, Phys. Rev. Lett. 88 (2002) 065501.
[22] H. Sahin, J. Sivek, S. Li, B. Partoens, F.M. Peeters, Phys. Rev. B 88 (2013) 045434.
[23] J. Ma, D. Alfè, A. Michaelides, E. Wang, Phys. Rev. B 80 (2009) 033407.
[24] J.C. Meyer, C. Kisielowski, R. Erni, M.D. Rossell, M.F. Crommie, A. Zettl, Nano Lett. 8 (2008) 3582.
[25] N. Chandra, S. Namilae, C. Shet, Phys. Rev. B 69 (2004) 094101.
[26] Y. Zhao, Y. Lin, B.I. Yakobson, Phys. Rev. B 68 (2003) 233403.
[27] T.C. Dinadayalane, J. Leszczynski, Chem. Phys. Lett. 434 (2007) 86.
[28] Q.E. Wang, F.H. Wang, J.X. Shang, Y.S. Zhou, J. Phys.: Condens. Matter 21 (2009) 485506.
[29] Y.H. Zhang, K.G. Zhou, X.C. Gou, K.F. Xie, H. Zhang, Y. Peng, Chem. Phys. Lett. 484 (2010) 266.
[30] S.F. Wang, Y. Yao, H.L. Zhang, R. Wang, Phys. Lett. A 375 (2011) 4109.
[31] J.F. Gao, J.F. Zhang, H.S. Liu, Q.F. Zhang, J.J. Zhao, Nanoscale 5 (2013) 9785.
[32] S.Y. Wang, L.Z. Tan, W.H. Wang, S.G. Louie, N. Lin, Phys. Rev. Lett. 113 (2014) 196803.
[33] Y. Dong, Y. He, Y. Wang, H. Li, Carbon 68 (2014) 742.
[34] A. Chanana, A. Sengupta, S. Mahapatra, J. Appl. Phys. 115 (2014) 034501.
[35] X.Y. Sun, R.N. Wu, R. Xia, X.H. Chu, Y.J. Xu, Appl. Phys. Lett. 104 (2014) 183109.
[36] K. Jin, H.Y. Xiao, Y. Zhang, W.J. Weber, Appl. Phys. Lett. 104 (2014) 203106.
[37] A. Manjanath, A.K. Singh, Chem. Phys. Lett. 592 (2014) 52.
[38] J. Zhao, H. Zeng, B. Li, J.W. Wei, J.W. Liang, J. Phys. Chem. Solids 77 (2015) 8.
[39] J.P. Perdew, K. Burke, M. Ernzerhof, Phys. Rev. Lett. 77 (1996) 3865.
[40] J. White, D. Bird, Phys. Rev. B 50 (1994) 4954.
[41] T.H. Fischer, J. Almlof, J. Phys. Chem. 96 (1992) 9768.
[42] H.J. Monkhorst, J.D. Pack, Phys. Rev. B 13 (1976) 5188.